J. Plasma Physics (1999), *vol.* 61, *part* 4, *pp.* 543–552. Printed in the United Kingdom

Stabilization of the kinetic internal kink mode by a sheared poloidal flow

HIROSHI NAITOU,[1] TOSHIMITSU KOBAYASHI[1] and SHINJI TOKUDA[2]

[1] Department of Electrical and Electronic Engineering, Yamaguchi University, Tokiwadai 2557, Ube 755-8611, Japan

[2] Department of Fusion Plasma Research, Naka Fusion Research Establishment, Japan Atomic Energy Research Institute, Naka, Ibaraki 311-0193, Japan

(Received 1 June 1998 and in revised form 31 August 1998)

The effects of a sheared poloidal flow on the $m = 1$ (poloidal mode number) and $n = 1$ (toroidal mode number) kinetic internal kink mode are simulated by the linearized version of the gyro-reduced MHD code, GRM3D-2F, based on a two-field and two-fluid gyro-reduced MHD model, including the kinetic effects of electron inertia and the perturbed electron pressure gradients along the magnetic field. A parameter study for different values of d_e (collisionless electron skin depth) with a fixed value of $\rho_s = 0$ (ion Larmor radius estimated by the electron temperature) shows that the smaller-d_e case, which has the smaller growth rate, is stabilized by the smaller sheared poloidal flow. When ρ_s is raised to $\rho_s > d_e$ for a fixed value of d_e, the instability is stabilized by the smaller shear flow compared with the case of $\rho_s < d_e$, although the growth rate without the flow is larger for $\rho_s > d_e$. Since d_e is very much less than the minor radius, and $\rho_s > d_e$ for the existing and future experiments, it is possible that even a quite small sheared poloidal flow may have a crucial influence on the kinetic internal kink mode.

1. Introduction

The physics of sawtooth oscillation in tokamaks is still far from completely understood. The suppression of the sawtooth crash, the sawtooth crash on a rapid time scale, and the physics of $q_0 < 1$ (where q_0 is the safety factor at the magnetic axis) after the sawtooth crash are some examples. It is believed that the nonlinear development of the $m = 1$ (poloidal mode number) and $n = 1$ (toroidal mode number) (collisionless) kinetic internal kink mode is closely related to the sawtooth oscillation.

For the numerical study of these phenomena, it is necessary to develop an extended MHD simulation model that is the kinetic extension of the conventional MHD model. The development of such an extended model and the simulation of kinetic MHD phenomena in fusion plasmas using massively parallel computers are among the main objects of the NEXT (Numerical EXperiment of Tokamak) project in JAERI that was begun in 1996 (Tokuda 1996). We have developed a gyrokinetic particle code (GYR3D) (Naitou et al. 1995, 1996) a gyro-reduced MHD code (GRM3D-2F) (Naitou et al. 1997) and a particle–fluid hybrid code (Hybrid3D)

(Tokuda et al. 1998). These three codes, which have the exact energy invariances, are based on the nonlinear gyrokinetic Vlasov–Poisson–Ampère system (Hahm et al. 1988) and/or its moment equations.

It is important to develop several codes with different orders of physical accuracy and to benchmark those codes for the same physical phenomena. The nonlinear phenomena of the kinetic $m = 1$ and $n = 1$ internal kink mode have been studied using GYR3D, GRM3D-2F and Hybrid3D. Fast full reconnection (collisionless magnetic reconnection) followed by a second phase in which the configuration with $q_0 < 1$ is re-formed has been observed by these three codes. (This two-step model of reconnection was first predicted by the simulation by Biskamp and Drake (1994).)

Although previous studies have concentrated on the unstable internal kink mode, the mode can be linearly or nonlinearly stabilized. The stabilization of the internal kink mode is related to the suppression of the sawtooth oscillation and to the partial reconnection model in which the unstable internal kink mode is saturated at low amplitude; the shifted core plasma coexists with the $m = 1$ island (quasi)stationarily. The partial reconnection model can explain the experimental results for $q_0 < 1$ after the sawtooth collapse if some physical model to explain the fast flattening of the density and temperature is introduced (Lichtenberg et al. 1992). It is therefore important to investigate the stabilization mechanism of the internal kink mode. There are many candidates for the stabilization of the internal kink mode, such as the effects of pressure gradient (Rogers and Zakharov 1995), energetic trapped ions (White et al. 1988), a flat current profile around the $q = 1$ magnetic surface, and a sheared poloidal flow. Stabilization of the collisional internal kink mode by a sheared poloidal flow was studied by Kleva (1992). Here we treat the collisionless case in which the kinetic effects of electrons are responsible for the destabilizing mechanism.

In this paper a linear stability analysis of the $m = 1$ and $n = 1$ kinetic internal kink mode with the sheared poloidal flow is performed using the GRM3D-2F code. A brief summary of the gyro-reduced MHD model is given in Sec. 2. The simulation results for the kinetic $m = 1$ and $n = 1$ internal kink mode with a sheared poloidal flow are presented in Sec. 3. Concluding remarks and a discussion are given in Sec. 4.

2. Gyro-reduced MHD model

We assume a rectangular system with dimensions L_x, L_y and L_z. There is a strong and constant magnetic field (toroidal magnetic field), $\mathbf{B}_T = B_0\mathbf{b}$, where $\mathbf{b}$ is the unit vector in the z direction. The compressional component of the longitudinal magnetic field is neglected in the low-β approximation. A periodic boundary condition is assumed in the z direction. The system is bounded by a perfectly conducting wall in the x and y (poloidal) directions.

The moment equations of the gyrokinetic Vlasov equations are used to derive the gyro-reduced MHD model. Because the terminology 'gyro-fluid' is usually used for the gyro-Landau model (Hammett and Perkins 1990; Waltz et al. 1992), we call our model 'gyro-reduced MHD' because it corresponds to the extension of the reduced MHD model given by Strauss (1976). This model is basically a two-fluid model; hence electron inertia as well as the electron pressure gradient along the magnetic field are included in the system of equations.

The gyro-reduced MHD model comprises two equations for the electrostatic po-

https://doi.org/10.1017/S0022377899007734 Published online by Cambridge University Press

tential ϕ and the z component of the vector potential A_z:

$$\frac{d}{dt}(\nabla_\perp^2 \phi) = -v_A^2\, \mathbf{b}^* \cdot \boldsymbol{\nabla}(\nabla_\perp^2 A_z)\,, \tag{1}$$

$$\frac{\partial}{\partial t} A_z = -\mathbf{b}^* \cdot \boldsymbol{\nabla}\phi + d_e^2\, \frac{d}{dt}(\nabla_\perp^2 A_z) + \rho_s^2\, \mathbf{b}^* \cdot \boldsymbol{\nabla}(\nabla_\perp^2 \phi)\,, \tag{2}$$

where $v_A = c\,\omega_{ci}/\omega_{pi}$ (with c the speed of light in vacuum, and ω_{ci} and ω_{pi} the ion cyclotron and plasma angular frequencies respectively) is the Alfvén velocity, $d_e = c/\omega_{pe}$ (with ω_{pe} the electron plasma angular frequency) is the collisionless electron skin depth, $\rho_s = (T_e/m_i)^{1/2}/\omega_{ci}$ (with m_i the ion mass and T_e the electron temperature) is the ion Larmor radius estimated in terms of the electron temperature, $\mathbf{b}^*$ is the unit vector of the magnetic field,

$$\mathbf{b}^* = \mathbf{b} + \frac{\boldsymbol{\nabla} A_z \times \mathbf{b}}{B_0}\,, \tag{3}$$

and d/dt is the convective derivative, defined by

$$\frac{d}{dt} = \frac{\partial}{\partial t} + \frac{\mathbf{b} \times \boldsymbol{\nabla}\phi}{B_0} \cdot \boldsymbol{\nabla}\,. \tag{4}$$

Equation (1) represents the vorticity equation, while the generalized Ohm's law in the direction parallel to the magnetic field is described by (2).

In order to derive (2), we have replaced the pressure term p_e in the electron moment equation by assuming $p_e = n_e T_e$ and T_e = constant (isothermal model);

$$\boldsymbol{\nabla} p_e = T_e \boldsymbol{\nabla} n_e = \frac{\epsilon_0 T_e}{e}\, \frac{\omega_{pi}^2}{\omega_{ci}^2}\, \boldsymbol{\nabla}(\nabla_\perp^2 \phi)\,, \tag{5}$$

where the gyrokinetic Poisson equation is used in the second equality by assuming $\delta n_i = 0$, which is consistent with assuming $U_i = 0$ (with U_i the ion fluid velocity parallel to the magnetic field) in the zeroth-order moment equation (continuity equation) of the ions.

3. Simulation results

The system is filled with a plasma with uniform equilibrium density and temperature. The equilibrium profile of A_z is chosen to be

$$A_z(x, y) = \frac{2 L_x L_y B_0}{\pi q_0 L_z} \sin\frac{\pi x}{L_x} \sin\frac{\pi y}{L_y}\,, \tag{6}$$

where q_0 is the safety factor at the magnetic axis. The q profile corresponding to the above A_z is given by (Strauss 1976)

$$q(x, y) = \frac{2}{\pi} q_0 K(\sin\psi), \tag{7a}$$

$$\cos\psi = \sin\frac{\pi x}{L_x} \sin\frac{\pi y}{L_y}\,, \tag{7b}$$

where K is the elliptic integral of the first kind. The value of q increases monotonically from the axis to the wall, where q is infinite. The central value of $q = q_0 = 0.85$ is selected for the equilibrium.

Figure 1 shows the equilibrium electrostatic potential profile given by

$$\phi(x, y) = \phi_0 \left(\sin\frac{\pi x}{L_x} \sin\frac{\pi y}{L_y}\right)^4\,. \tag{8}$$

https://doi.org/10.1017/S0022377899007734 Published online by Cambridge University Press

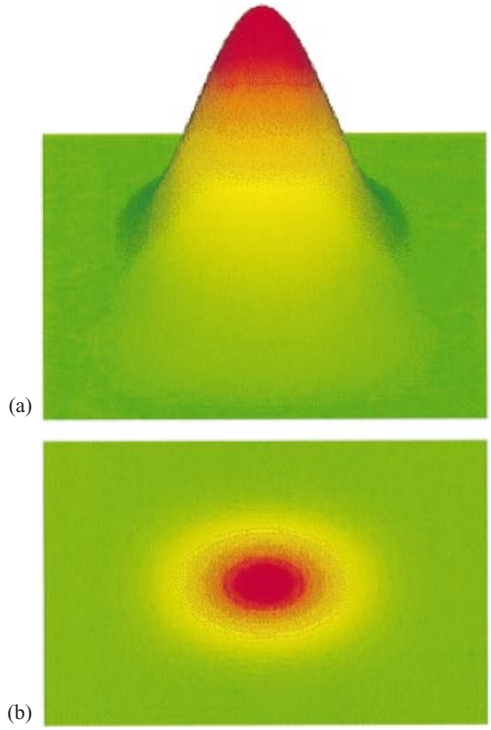

Figure 1. The equilibrium profile of the electrostatic potential $\phi(x, y)$: (a) three-dimensional view; (b) two-dimensional view.

The profile of the sheared poloidal flow, which is generated by the $\mathbf{E} \times \mathbf{B}$ drift due to the radial electric field $(-\boldsymbol{\nabla}\phi)$ and the toroidal magnetic field, is presented in Fig. 2. Note that the sheared flow velocity used in the calculation is much less than the poloidal Alfvén velocity.

The simulation was performed using the linearized version of the GRM3D-2F code, which includes only $n = \pm 1$ modes in addition to the equilibrium $n = 0$ mode. A two-dimensional 256×256 mesh is used for the numerical calculation because the modes are expressed in Fourier series in the z-direction. The equations were solved by a pseudospectral method. A filtering technique in Fourier space was employed to reduce the highest-wavenumber modes. The smoothing function for the filtering was selected so as not to change the linear growth rate. No other artificial techniques such as a numerical viscosity were utilized.

The cases without a sheared poloidal flow were studied by Naitou et al. (1997). It was found that the dependence of the growth rates on d_e and ρ_s agrees with the theory of Zakharov et al. (1993):

$$\gamma \sim \begin{cases} 2\pi q' d_e \dfrac{v_A}{L_z} & (d_e \gg \rho_s), \quad (9) \\ 2\pi q' d_e^{1/3} \rho_s^{2/3} \dfrac{v_A}{L_z} & (d_e \ll \rho_s), \quad (10) \end{cases}$$

where $q' = dq/dr$.

The linear mode structures for the cases with and without a sheared poloidal flow are compared in Figs 3 and 4. For both cases, $d_e = 12\Delta$ and $\rho_s = 0$ were chosen,

https://doi.org/10.1017/S0022377899007734 Published online by Cambridge University Press

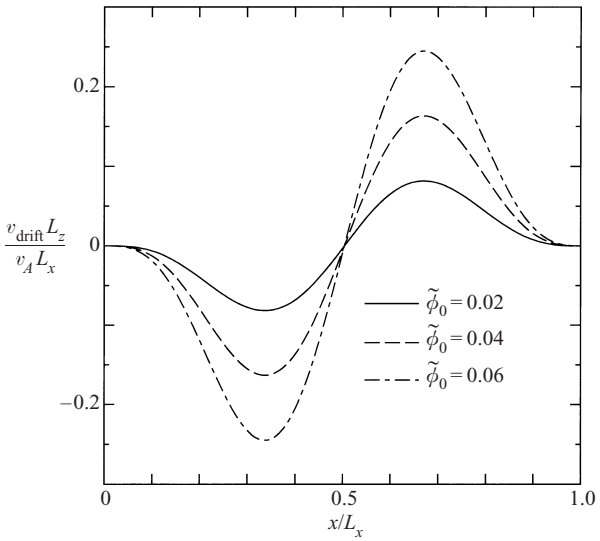

Figure 2. The profile of the sheared poloidal flow: the y component of the $\mathbf{E} \times \mathbf{B}$ drift velocity estimated at $y = \frac{1}{2} L_y$ and $0 < x < L_x$.

where Δ denotes the width of the spatial mesh. Figure 3 represents the typical mode structures of the pure $m = 1$ and $n = 1$ kinetic internal kink mode. We can see the dipole potential profile in Fig. 3(a). Figure 3(b) shows a negative current-density layer on the semicircle of the $q = 1$ surface as well as a positive layer on the semicircle at the opposite side. Both layers have width of order d_e. A thin $m = 1$ double-layer profile of the charge density is observed in Fig. 3(c); the positive layer faces the negative layer across the surface $q = 1$. When a sheared poloidal flow with $\tilde{\phi}_0 = 0.04$ is added, where $\tilde{\phi}$ is the normalized electrostatic potential defined by $(L_z/v_A L_x^2 B_0)\phi$, the mode structures of Fig. 3 are deformed as shown in Fig. 4. Here the mode structures are rotating in the poloidal direction. The growth rate for the case $\tilde{\phi}_0 = 0.04$ is $0.33\, v_A/L_z$, which is smaller than the value of $\gamma = 0.39\, v_A/L_z$ for the case without a sheared flow. Although the rigid rotation of the mode does not affect the mode structure, the difference in the poloidal angular velocity tends to modify the typical mode structure of the internal kink mode, and hence has a stabilizing effect. The case with a sheared flow has a finer mode structure in the radial direction; a finer mesh is required to resolve such a mode structure.

Figure 5 summarizes the $\tilde{\phi}_0$ dependence of the linear growth rate. To see the effects of d_e on the growth rate, we have fixed $\rho_s = 0$. It is clear that a sheared poloidal flow has a stabilizing effect on the kinetic internal kink mode. When the growth rate is small, i.e. d_e is small with $\rho_s = 0$ (see (9)), the unstable mode is stabilized by a lower value of $\tilde{\phi}_0$. This result is different from the case of a resistive internal kink mode, in which stabilization ocurs at a fixed value of the sheared flow in spite of the growth rate (i.e. resistivity) (Kleva 1992). Figure 6 shows the $\tilde{\phi}_0$ dependence of the linear growth rate for $\rho_s = 0$ and $\rho_s = 16\Delta$ for a fixed value of $d_e = 8\Delta$. The growth rate without a sheared flow is higher for larger values of ρ_s when $\rho_s > d_e$ (see (9) and (10)). The instability, however, is stabilized by a small value of $\tilde{\phi}_0$ for $\rho_s > d_e$.

https://doi.org/10.1017/S0022377899007734 Published online by Cambridge University Press

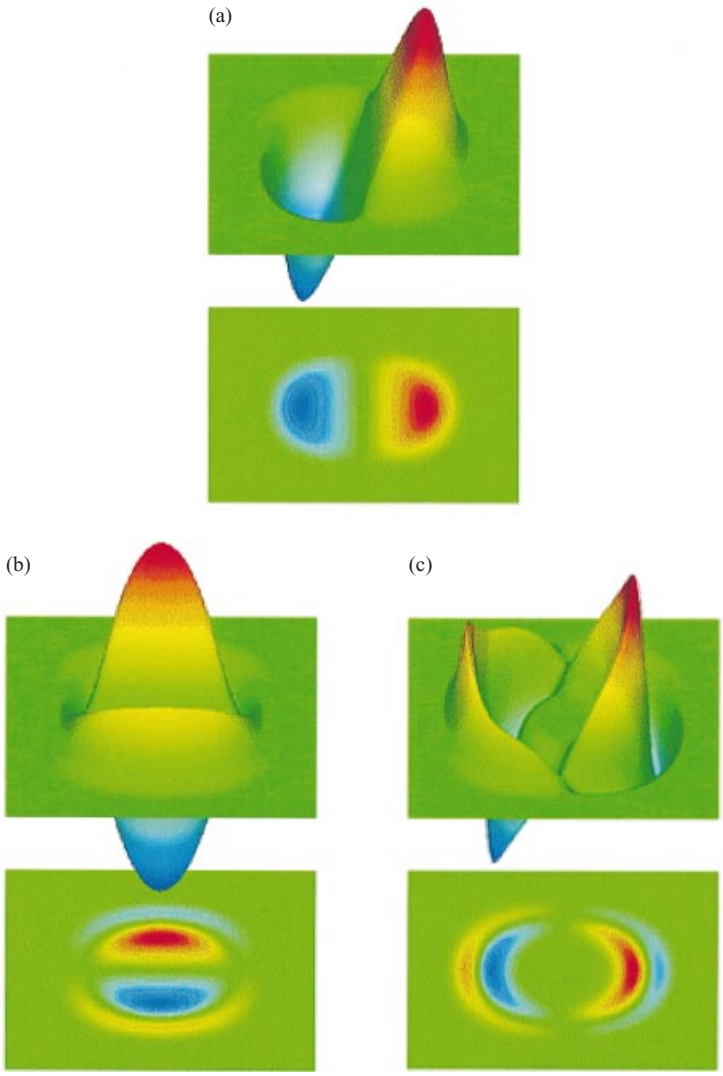

Figure 3. The linear mode structure at the poloidal cross-section $z = 0$ without a sheared poloidal flow for (a) the electrostatic potential, (b) the current density, and (c) the charge density. Here $d_e = 12\Delta$ and $\rho_s = 0$.

4. Conclusions and discussion

A linear stability analysis of the $m = 1$ and $n = 1$ kinetic internal kink mode with a sheared poloidal flow has been performed using the linearized version of GRM3D-2F, which is a two-field and two-fluid gyro-reduced MHD code including the kinetic effects of electron inertia and the perturbed electron pressure gradients along the magnetic field. The numerical results verify that the unstable kinetic internal kink mode is stabilized by a sheared poloidal flow with typical velocity less than the poloidal Alfvén velocity. The stress due to the differential angular velocity of the flow deforms the typical mode structure of the pure internal kink mode, and hence has a stabilizing effect.

https://doi.org/10.1017/S0022377899007734 Published online by Cambridge University Press

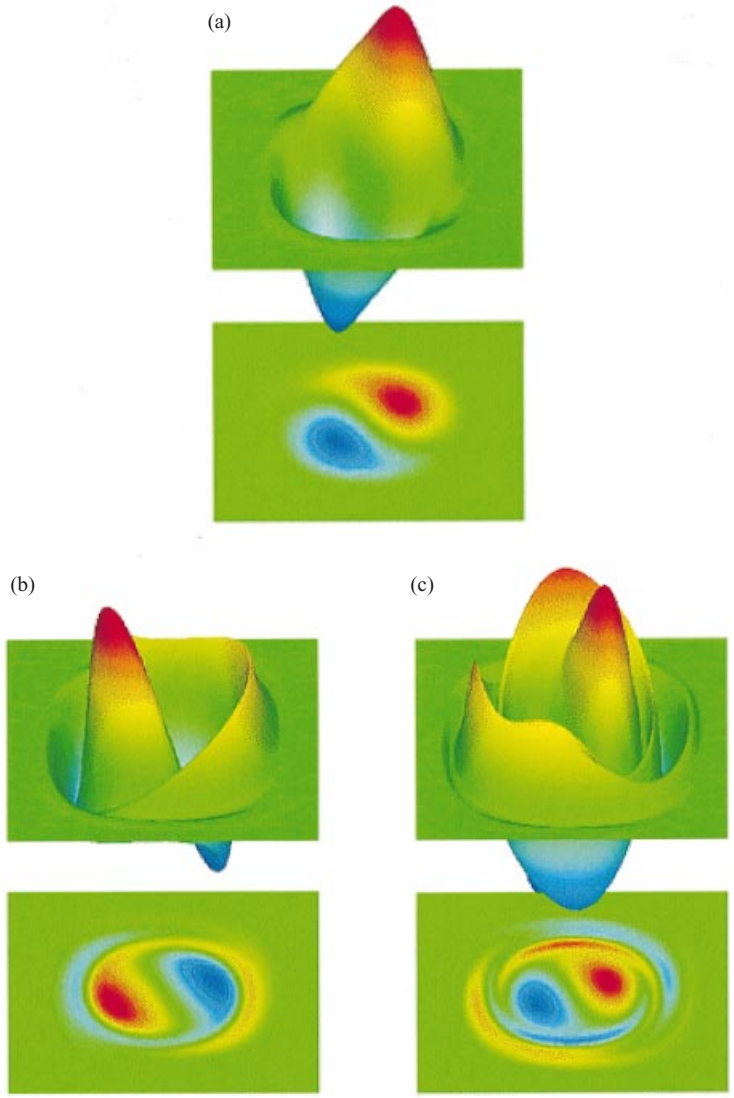

Figure 4. The linear mode structure at the poloidal cross-section $z = 0$ with a sheared poloidal flow with $\tilde{\phi}_0 = 0.04$ for (a) the electrostatic potential, (b) the current density and (c) the charge density. Here $d_e = 12\Delta$ and $\rho_s = 0$.

A parameter study for different values of d_e with a fixed value of $\rho_s = 0$ shows that the smaller-d_e case, which has the smaller growth rate, is stabilized by a smaller sheared poloidal flow. Note that the growth rate without flow is proportional to d_e/L_x or d_e/a (a is the minor radius) for $d_e > \rho_s$. We can see that the parameter study performed here is limited to relatively large values of d_e/a because of the limitation of computer resources, although $d_e/a \ll 1$. Therefore a further parameter study is needed in order to know whether this tendency can be extrapolated to the case of much smaller d_e/a corresponding to a tokamak experiment. When ρ_s is increased so that $\rho_s > d_e$ for a fixed value of d_e, the instability is stabilized by a smaller shear flow compared with the case of $\rho_s < d_e$, although the growth rate

https://doi.org/10.1017/S0022377899007734 Published online by Cambridge University Press

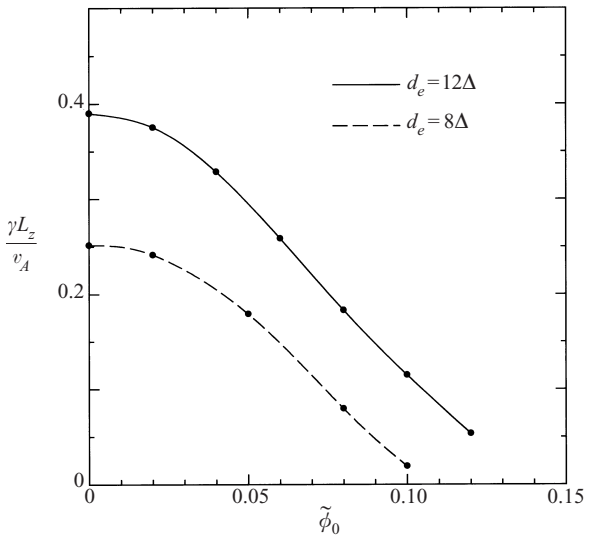

Figure 5. The growth rate as a function of the strength of the sheared poloidal flow, $\tilde{\phi}_0$. The cases of $d_e = 8\Delta$ and $d_e = 12\Delta$ are shown, for a fixed value of $\rho_s = 0$. A $256\Delta \times 256\Delta$ mesh has been used.

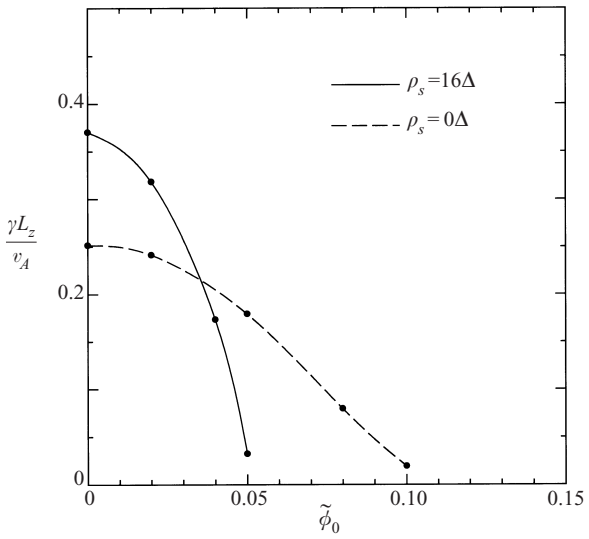

Figure 6. The growth rate as a function of the strength of the sheared poloidal flow, $\tilde{\phi}_0$. The cases of $\rho_s = 0$ and $\rho_s = 16\Delta$ are shown for a fixed value of $d_e = 8\Delta$. A $256\Delta \times 256\Delta$ mesh has been used.

without a poloidal shear flow is larger for the case of $\rho_s > d_e$. Since d_e/a is very much less than unity, and $\rho_s > d_e$ for existing and future experiments, it is possible that even a small sheared poloidal flow (i.e. a small radial electric field) may have a dominant influence on the kinetic internal kink mode.

The effects of $\mathbf{E} \times \mathbf{B}$ velocity shear on turbulence and transport in magnetic confinement devices have been widely discussed. The rough criterion for the stability of the unstable mode (or suppression of turbulence and transport) is that the $\mathbf{E} \times \mathbf{B}$

https://doi.org/10.1017/S0022377899007734 Published online by Cambridge University Press

shear rate is greater than the growth rate without the $\mathbf{E}\times\mathbf{B}$ velocity shear (Burrell 1997). Here we compare this criterion with the simulation results. The $\mathbf{E}\times\mathbf{B}$ shear rate for flute-like modes is defined by the following equation (Hahm and Burrell 1995):

$$\omega_E = \frac{L_r}{L_\theta}\frac{(RB_\theta)^2}{B}\frac{\partial^2\phi}{\partial\psi^2}\,, \tag{11}$$

where L_r and L_θ are the correlation lengths of the mode in the radial and poloidal directions respectively, B_θ is a poloidal magnetic field and ψ is the poloidal flux function. Note that the flux function ψ is RA_z (where $R = L_z/2\pi$) for our case. Approximating $B_\theta \approx rB_0/Rq$ and $B \approx B_0$, we have the following estimate for ω_E at the $q = 1$ rational surface:

$$\omega_E \approx 26.4\frac{L_r}{L_\theta}\tilde{\phi}_0\frac{v_A}{L_z}\,. \tag{12}$$

The growth rate without a sheared poloidal flow for the case of $d_e = 8\Delta$ and $\rho_s = 0$ is $\gamma = 0.25v_A/L_z$. This case is stabilized when $\tilde{\phi}_0 \approx 0.1$. We may approximate L_θ by r_0, where r_0 is the minor radius of the $q = 1$ magnetic surface. There are two choices for the estimation of L_r. When the radial extent of the layer at the $q = 1$ surface, d_e, is used for L_r, we have $\omega_E \approx 0.33v_A/L_z$ which is slightly greater than γ. If we approximate L_r by r_0 we have $\omega_E \approx 2.6v_A/L_z$, which is much greater than γ. While the former estimate of ω_E cannot explain the d_e dependence (for $\rho_s = 0$) of the simulation results, the latter estimate can. It is possible that the former estimate may explain the ρ_s dependence for $\rho_s > d_e$ if we use $L_r \approx \rho_s$. The latter estimate, however, cannot explain the ρ_s dependence. These differences between the criterion and the simulation results may come from the fact that we used only the local value of ω_E, although a internal kink mode is a global mode. Anyway, further study is needed before drawing a decisive conclusion.

The study in this paper has been limited to a linear mode analysis. A nonlinear simulation of the $m = 1$ and $n = 1$ kinetic internal kink mode with a sheared poloidal flow using the nonlinear version of the GRM3D-2F is the subject of a forthcoming paper. Also, a comparison of the simulation results from the GRM3D-2F, GYR3D and Hybrid3D codes will be reported in the near future.

Acknowledgements

The authors are grateful to Professor O. Fukumasa (Yamaguchi University). They also express their thanks to Drs M. Azumi, M. Yamagiwa and T. Matsumoto (JAERI), Professors T. Sato and T. Kamimura (National Institute for Fusion Science), Professor W. W. Lee (Princeton Plasma Physics Laboratory), Professor V. K. Decyk (University of California at Los Angeles), and Professor R. D. Sydora (University of Alberta). The Fujitsu VPP500 at JAERI Tokai Institute and NEC SX-4 at the National Institute for Fusion Science were used for the numerical calculation.

References

Biskamp, D. and Drake, J. F. 1994 *Phys. Rev. Lett.* **73**, 971.
Burrell, K. H. 1997 *Phys. Plasmas* **4**, 1499.
Hahm, T. S. and Burrell, K. H. 1995 *Phys. Plasmas* **2**, 1648.
Hahm, T. S., Lee, W. W. and Brizard, A. 1988 *Phys. Fluids* **31**, 1940.
Hammett, G. W. and Perkins, F. W. 1990 *Phys. Rev. Lett.* **64**, 3019.

Kleva, R. G. 1992 *Phys. Fluids* **B4**, 218.
Lichtenberg, A. J., Itoh, K., Itoh, S.-I. and Fukuyama, A. 1992 *Nucl. Fusion* **32**, 495.
Naitou, H., Tsuda, K., Lee, W. W. and Sydora, R. D. 1995 *Phys. Plasmas* **2**, 4257.
Naitou, H., Sonoda, T., Tokuda, S. and Decyk, V. K. 1996 *J. Plasma Fusion Res.* **72**, 259.
Naitou, H., Kitagawa, H. and Tokuda, S. 1997 *J. Plasma Fusion Res.* **73**, 174.
Rogers, B. and Zakharov, L. 1995 *Phys. Plasmas* **2**, 3420.
Strauss, H. R. 1976 *Phys. Fluids* **19**, 134.
Tokuda, S. 1996 *J. Plasma Fusion Res.* **72**, 916 [in Japanese].
Tokuda, S., Naitou, H. and Lee, W. W. 1998 *J. Plasma Fusion Res.* **74**, 44.
Waltz, R. E., Dominguez, R. R. and Hammett, G. W. 1992 *Phys. Fluids* **B4**, 3138.
White, R. B., Rutherford, P. H., Colestock, P. and Bussac, M. N. 1988 *Phys. Rev. Lett.* **60**, 2038.
Zakharov, L., Rogers, B. and Migliuolo, S. 1993 *Phys. Fluids* **B5**, 2498.